JOURNAL OF SYNCHROTRON RADIATION

Volume 28 (2021)

Supporting information for article:

New high-throughput endstation to accelerate the experimental optimization pipeline for synchrotron X-ray footprinting

Rohit Jain, Donald Abel, Maksim Rakitin, Michael Sullivan, David T. Lodowski, Mark R. Chance and Erik R. Farquhar

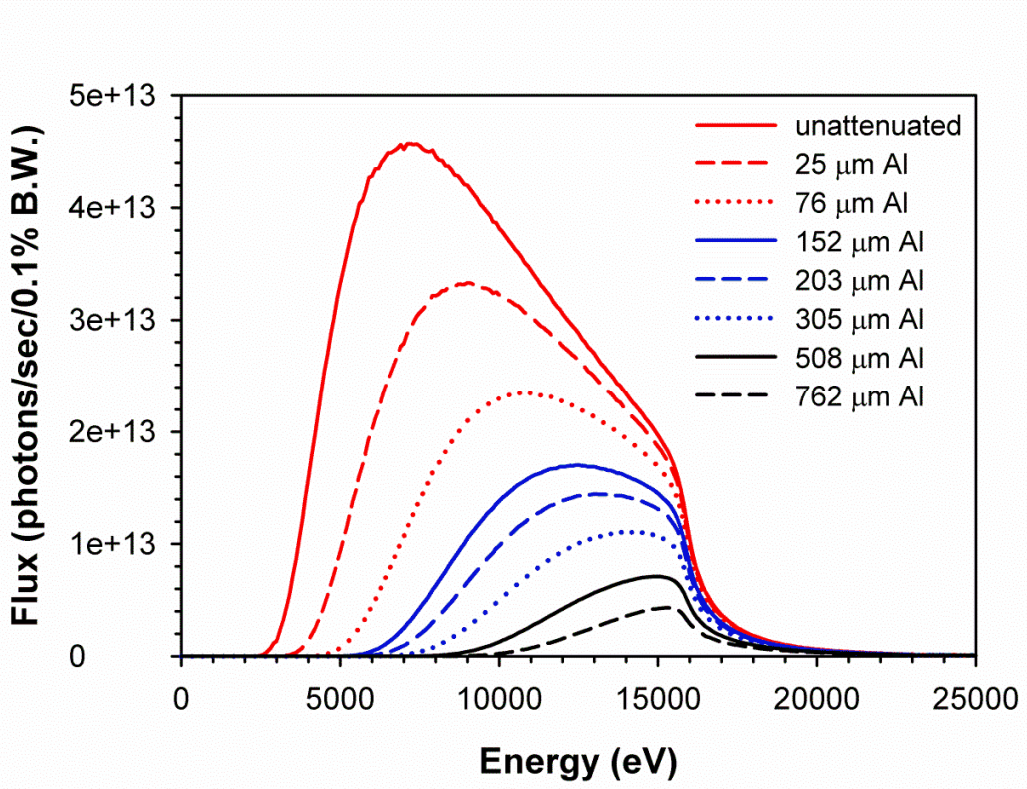

Figure S1 XFP flux curves (calculated for 500 mA NSLS-II ring current) as a function of aluminum attenuation, for a location just after the attenuator wheel.

Table S1 Effect of Aluminum Attenuation on Calculated XFP Beam Power.

Aluminum Thickness (μm)	Power after Attenuator (W) [a]	Power Incident on Sample (W) [b]
0	66.8	51.0
25	47.8	40.0
76	31.6	28.1
152	20.7	19.0
203	16.5	15.3
305	11.2	10.5
508	6.0	5.7
762	3.1	3.0

[a] Calculated for 500mA NSLS-II ring current for power transmitted through selected attenuator after correcting for absorption by 254 μm Be, Rh-coated mirror at 4.2 mrad angle, and 100 μm diamond.

[b] Calculated for 500mA NSLS-II ring current after further correcting for effects of 141 μm diamond (diamond beam imaging diagnostic), 50 cm He flight path, and a 25 μm Kapton exit window.

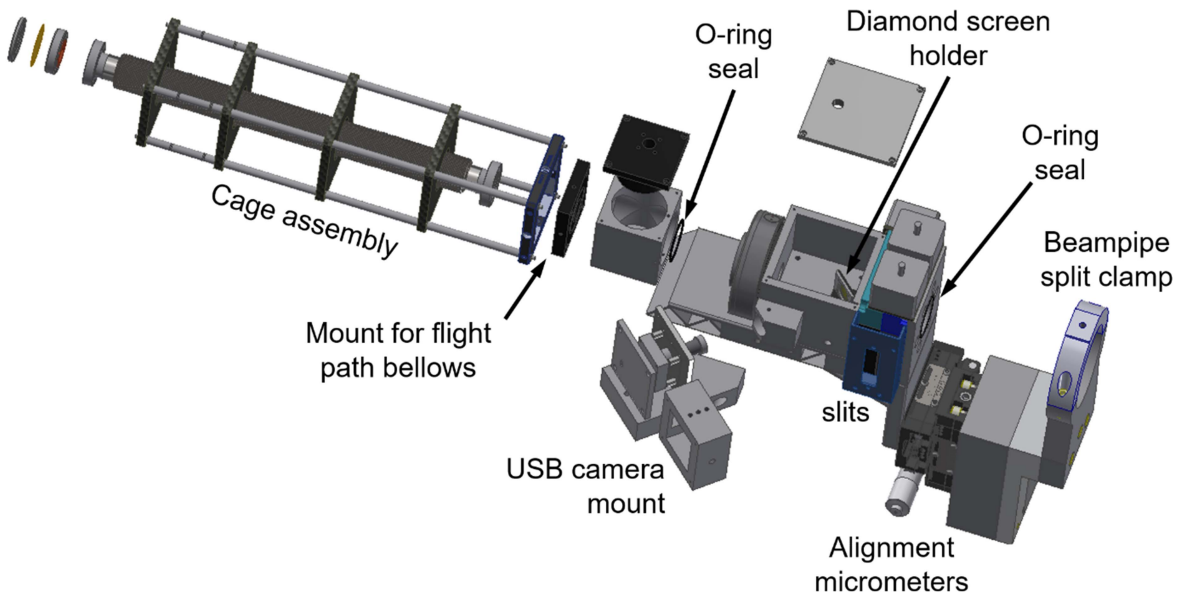

Figure S2 Exploded top-down view of the assembly that provides X-ray beam attenuation, images the X-ray beam, and supports the Uniblitz fast shutter for the high-throughput endstation, highlighting interior components of the assembly not visible in Figure 2, such as the diamond screen holder and sealing o-rings.

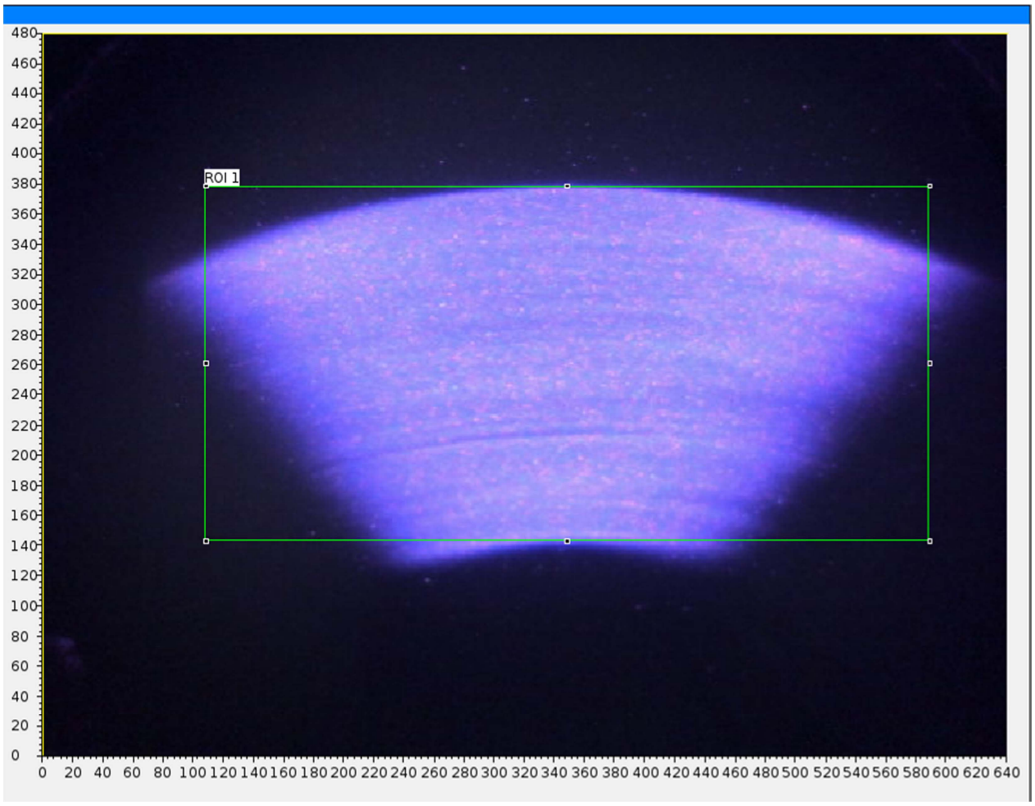

Figure S3 Image of the XFP pink beam seen on the diamond screen in the beam imaging module, viewed using a color USB camera. The green box indicates a region of interest that can be used to monitor X-ray beam position and stability during experiments.

Table S2 Fits to Alexa488 Rate Decay vs. Concentration Plots for a Footprinting Compound Library.

Category	Compound	Application	Exp. fit	decay const. high conc.[a]	decay const. low conc.[a]	R^2
Protein	Lysozyme	Protein	Double	0.28 ± 0.04	2.58 ± 0.81	0.99
Buffer	Citrate	Protein stability	Double	0.71 ± 0.22	5.00 ± 3.38	0.99
Buffer	$NH_4CH_3CO_2$	Protein stability	Single	-	3.27 ± 3.38	0.99
Buffer	Tris	Protein stability	Single	0.78 ± 0.07	-	0.99
Buffer	MES	Protein stability	Single	0.21 ± 0.04	-	0.97
Detergent	LMNG	Membrane proteins	Double	0.05 ± 0.02	0.47 ± 0.23	0.99
Detergent	DDM	Membrane proteins	Double	0.15 ± 0.01	0.87 ± 0.01	0.91
Denaturant	Urea	Protein folding	Single	0.97 ± 0.09	-	0.99
Denaturant	GdnHCl	Protein folding	Single	0.58 ± 0.11	-	0.97
Sugar	Glucose	Protein ligand studies	Double	0.28 ± 0.09	3.66 ± 1.57	0.98
Sugar	Sucrose	Protein ligand studies	Double	0.34 ± 0.01	5.66 ± 1.23	0.99
Nucleotides	ATP	Enzyme catalysis	Single	-	0.31 ± 0.01	0.99
Nucleotides	GDP	Enzyme catalysis	Double	0.02 ± 0.01	0.20 ± 0.04	0.99
Nucleotides	dNTPs	Enzyme catalysis	Double	0.02 ± 0.01	0.11 ± 0.05	0.99
Reducing agent	DTT	Disulfide bond reduction	Double	0.08 ± 0.05	0.76 ± 0.45	0.98
Reducing agent	TCEP	Disulfide bond reduction	Double	0.18 ± 0.02	4.73 ± 0.52	0.99
Reducing agent	β-ME	Disulfide bond reduction	Double	0.004 ± 0.001	0.04 ± 0.01	0.99
Organic solvent	Acetonitrile	Protein drug interaction	Double	0.41 ± 0.13	2.43 ± 0.81	0.99
Organic solvent	Methanol	Protein drug interaction	Double	0.001 ± 0.001	0.009 ± 0.002	0.99
Organic solvent	DMSO	Protein drug interaction	Double	0.001 ± 0.001	0.006 ± 0.001	0.99
Purification	Imidazole	Protein purification	Single	-	0.23 ± 0.04	0.97
Purification	Biotin	Protein purification	Double	0.012 ± 0.002	0.12 ± 0.001	0.99
Storage	Glycerol	Protein stability	Double	0.001 ± 0.001	0.015 ± 0.003	0.99

[a] Errors are those reported from the non-linear least squares fit to either a single or double exponential decay function.